Rapid Communications

Aperiodic topological crystalline insulators

Huaqing Huang,[1] Yong-Shi Wu,[2,3] and Feng Liu[1,*]

[1]*Department of Materials Science and Engineering, University of Utah, Salt Lake City, Utah 84112, USA*

[2]*Department of Physics and Astronomy, University of Utah, Salt Lake City, Utah 84112, USA*

[3]*State Key Laboratory of Surface Physics and Department of Physics, Fudan University, Shanghai 200443, China*

(Received 27 April 2019; published 6 January 2020)

Topological crystalline insulators (TCIs) are usually described with topological protection imposed by the crystalline symmetry. In general, however, the existence of TCI states does not necessitate the periodicity of crystals as long as an essential lattice symmetry can be identified. Here we demonstrate the compatibility of TCIs with aperiodic systems, as exemplified by an octagonal quasicrystal. The aperiodic TCIs we proposed are attributed to a band inversion mechanism, which inverts states with the same parity but opposite eigenvalues of a specific symmetry (such as mirror reflection). The nontrivial topology is characterized by a nonzero integer "mirror Bott index." Moreover, we demonstrate that the topological edge states and quantized conductance of the aperiodic TCI, which are robust against disorder, can be effectively manipulated by external electric fields. Our findings not only provide a better understanding of electronic topology in relation to symmetry but also extend the experimental realization of topological states to much broader material categories beyond crystals.

DOI: 10.1103/PhysRevB.101.041103

Topological crystalline insulators (TCIs) [1] represent the states of matter in which the topological order of electronic structures arises from generic crystalline symmetries instead of time-reversal symmetries as for topological insulators (TIs) [2–4]. There are many proposed TCI phases depending on different crystalline symmetries [5–13]. Recently, a theory of symmetry-based indicator [14] has been established to diagnose underlying band topology of a large amount of crystalline materials [15–17]. Yet those relying on mirror symmetry [18,19] are of particular interest, as they have been experimentally observed [20–24] or theoretically predicted [25–31] in various three-dimensional (3D) as well as two-dimensional (2D) materials [32–38]. So far, almost all the existing TCIs are based on crystalline solids. In general, however, the existence of TCIs does not necessarily require the periodicity of crystals as long as an essential lattice symmetry can be identified. Here, we propose the realization of TCIs in aperiodic structures [39–41], such as quasicrystals, by considering a band inversion mechanism which inverts states with the same party but opposite eigenvalues of the identified symmetries.

Beyond the classical crystallographic restriction of periodicity, we introduce the concept of aperiodic TCIs, as exemplified by an octagonal quasicrystal. We show that the aperiodic TCI can be realized by considering a band inversion between states with opposite mirror eigenvalues for a specific reflection operation. We characterize its nontrivial topology by deriving a topological invariant, the mirror Bott index, in addition to the conventional signatures of robust edge states and quantized transport as in crystals. Moveover, we found that the topological edge states of the aperiodic TCI can be gapped by applying a perpendicular electric field and the system can even become a quantum spin Hall (QSH) insulator by further increasing the electric field strength. Our work opens another direction in the theoretical studies of aperiodic matters with different topological classes and in the experimental realization of topological quantum matters beyond common crystalline materials.

We first illustrate the general band inversion to provide an alternative view of TCI in terms of symmetries of states that underlines the band inversion, which will be especially useful to *a priori* design/search TCIs based on simple orbital analysis. The band inversion provides an intuitive physical picture to understand topological states which was actually discovered long before the concept of topological insulators [42–44]. Generally, the nontrivial electronic topology involves parity-invoked band inversions (PBIs) which invert band-edge states with opposite parities [2–4]. Typically, an odd number of PBIs give rise to TIs (e.g., HgTe quantum wells) [45,46], and an even number of leads to TCIs (e.g., SnTe bulk and films) [18,32,47]. In contrast, a band inversion between states with the same parity but different other symmetry eigenvalues can also give rise to symmetry-protected topological states, i.e., the TCIs. Specifically, we focus on the in-plane mirror symmetry of 2D systems. For example, although all three p orbitals have odd parities, band-edge states composed of a p_z orbital are antisymmetric (odd) but those composed of p_x and p_y orbitals are symmetric (even) about the x-y mirror plane. As such, the p_z-$p_{x,y}$ band inversion will give rise to TCI states, as elaborated below. This band inversion mechanism for TCIs is general, applicable to other orbtials (such as d), and both periodic and aperiodic systems.

We demonstrate the realization of aperiodic TCIs using a generic atomic-basis model on 2D quasicrystals, such as the octagonal Ammann-Beenker tiling [48–50] shown in Fig. 1(a). There are three orbitals (p_x, p_y, and p_z) per site having opposite eigenvalues with respect to the mirror operation

*Corresponding author: fliu@eng.utah.edu

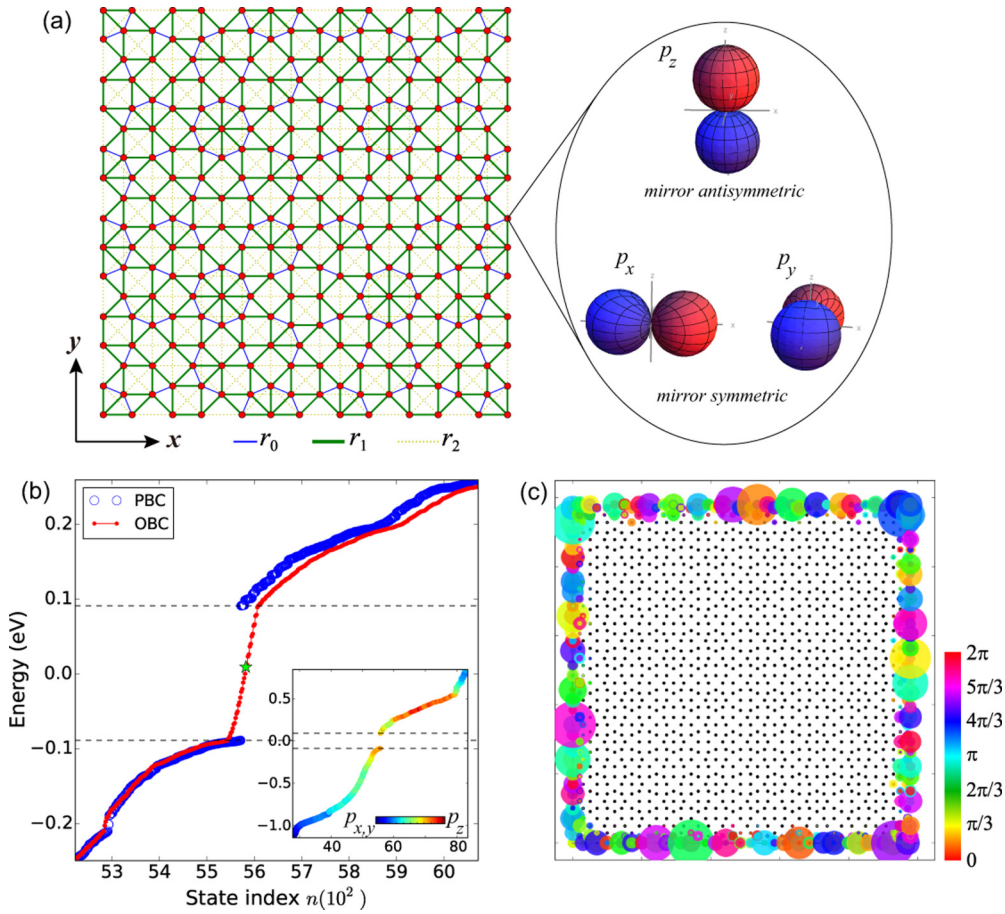

FIG. 1. (a) Octagonal quasicrystal lattice based on the Ammann-Beenker tiling containing 264 vertices. Three atomic p orbitals with different mirror symmetries are placed on vertices. r_0, r_1, and r_2 denote the first three nearest-neighbor distances. (b) Energy eigenvalues E_n versus the state index n from the calculation of a quasicrystal sample with 1393 atoms (three orbitals and two spins on each atom). The parameters used here are $\epsilon_{p_z} = -0.86$, $\epsilon_{p_{x,y}} = -1.86$, $V_{pp\sigma} = 0.49$, $V_{pp\pi} = -0.15$, and $\lambda = 1.25$ eV (see Supplemental Material [53]). The inset shows the orbital-resolved spectrum of the quasicrystal with a PBC. (c) The wave function $|\psi(\mathbf{r})\rangle = \chi(\mathbf{r})e^{i\phi(\mathbf{r})}$ of the midgap state [marked as the green star in (a)] is located on the edge. The size and the color of the blob indicates the amplitude $|\chi(\mathbf{r})|^2$ and phase $\phi(\mathbf{r})$ of the wave function, respectively.

$\hat{M}_z$. The Hamiltonian is given by

$$H = \sum_{i\alpha\mu} \epsilon_\alpha c^\dagger_{i\alpha\mu} c_{i\alpha\mu} + \sum_{\langle i\alpha, j\beta\rangle, \mu} t_{i\alpha, j\beta} c^\dagger_{i\alpha\mu} c_{j\beta\mu} + i\lambda \sum_{i,\mu\nu} (\mathbf{c}^\dagger_{i\mu} \times \mathbf{c}_{i\nu}) \cdot \mathbf{s}_{\mu\nu}, \quad (1)$$

where $c^\dagger_{i\alpha\mu}$ are electron creation operators on the $\alpha(= p_x, p_y, p_z)$ orbital with spin $\mu(=\uparrow, \downarrow)$ at the ith site. ϵ_α is the on-site energy of the α orbital. $t_{i\alpha, j\beta} = t_{\alpha\beta}(\mathbf{r}_{ij})$ is the Slater-Koster hopping integral which depends on orbital types and the intersite vector $\mathbf{r}_{ij}$ from sites i to j [51,52]. λ is the spin-orbit coupling (SOC) strength, $\mathbf{c}^\dagger_{i\mu} = (c^\dagger_{ip_x}, c^\dagger_{ip_y}, c^\dagger_{ip_z})_\mu$, and $\mathbf{s} = (\sigma_x, \sigma_y, \sigma_z)$ are the Pauli matrices. Since only the band inversion between the $p_{x,y}$ and p_z states of different mirror eigenvalues is important for the realization of TCIs, we focus mainly on 2/3 filling of electron states hereafter (see Supplemental Material [53]).

We numerically studied the octagonal quasicrystal with an artificial periodic boundary condition (PBC) and an open boundary condition (OBC), respectively. As shown in Fig. 1(b), the PBC system shows an energy gap, while a set of energy eigenvalues appears in the gap region for the OBC system. Interestingly, the wave function of a typical midgap state distributes on the boundary of the finite quasicrystal sample, implying that it is an "edge state," as displayed in Fig. 1(c). Further studies indicate that these edge states are robustly localized on the boundaries regardless of the edge geometries of the finite samples [53]. The existence of bulk energy gap and robust midgap edge states, which are known manifestations of the QSH state [54–56], suggest a nontrivial electronic topology. In order to examine the $\mathbb{Z}_2$ topology of the quasicrystal, we first calculated the spin Bott index B_s, a topological invariant for the QSH states in noncrystalline systems [55]. However, the calculated spin Bott index is $B_s = 0$, indicating that it is not a QSH insulator.

Remarkably, the orbital-resolved PBC spectrum exhibits signatures of a band inversion between p_z and $p_{x,y}$ orbitals [see inset of Fig. 1(b)], implying a nontrivial "crystalline" electronic topology in the aperiodic system. As a planar 2D structure, the quasicrystal naturally possesses an in-plane mirror symmetry. After further inspection, it turns out that the above edge states are topologically protected by the

in-plane mirror symmetry. Therefore, this "aperiodic" system is actually a mirror-protected TCI instead of a time-reversal-protected QSH insulator, as elaborated below.

It is well known that for a crystal with mirror symmetry, the mirror operator $\hat{M}_z$ commutes with the Hamiltonian: $[H, \hat{M}_z] = 0$. One can divide the wave functions in the mirror-invariant plane of the Brillouin zone into two separate sets according to their eigenvalues ($\pm i$) and calculate their respective Chern numbers $C_{\pm i}$. The mirror Chern number, which is defined as $C_m = (C_{+i} - C_{-i})/2$, gives a $\mathbb{Z}$ classification for the band topology of the crystalline systems [57]. Following the similar idea and based on the significant development of real-space formulations of topological invariants [58–68], here we straightforwardly derive an alternative topological invariant, the mirror Bott index, to determine the mirror-protected TCI state in aperiodic systems.

To do so, we first construct the projected mirror operator,

$$P_m = P\hat{M}_z P, \tag{2}$$

where $P = \sum_j^{N_{\rm occ}} |\psi_j\rangle\langle\psi_j|$ is the projector operator to the occupied states and $\hat{M}_z = -i\sigma_z \otimes m_z$ with the Pauli matrix σ_z and $m_z = \mathrm{diag}(1, 1, -1)$ being the mirror matrices in the spin and orbital spaces, respectively. By solving the eigenvalue problem of P_m and constructing new projector operators $P_{\pm i}$,

$$P_m|\phi_j^{\pm}\rangle = \pm i|\phi_j^{\pm}\rangle, \tag{3}$$

$$P_{\pm i} = \sum_j^{N_{\rm occ}/2} |\phi_j^{\pm}\rangle\langle\phi_j^{\pm}|, \tag{4}$$

one can make a smooth decomposition $P = P_{+i} \oplus P_{-i}$ for two sectors with opposite mirror eigenvalues.

Next, we calculate the projected position operators

$$U_{\pm i} = P_{\pm i} e^{i2\pi X} P_{\pm i} + (I - P_{\pm i}), \tag{5}$$

$$V_{\pm i} = P_{\pm i} e^{i2\pi Y} P_{\pm i} + (I - P_{\pm i}), \tag{6}$$

where X and Y are the rescaled coordinates defined in the interval [0,1). The Bott index, which measures the commutativity of the projected position operators [58,59,64], are given by [69]

$$B_{\pm i} = \frac{1}{2\pi}\mathrm{Im}\{\mathrm{tr}[\log(V_{\pm i}U_{\pm i}V_{\pm i}^{\dagger}U_{\pm i}^{\dagger})]\}, \tag{7}$$

for the two mirror sectors, respectively. Finally, we define the mirror Bott index as the half difference between the Bott indices for the two mirror sectors

$$B_m = \tfrac{1}{2}(B_{+i} - B_{-i}). \tag{8}$$

We checked the above definition for both crystalline and disordered systems with respect to mirror symmetry and confirm the mirror Bott index is equivalent to the mirror Chern number for crystals [53]. This proves that the mirror Bott index is a well-defined topological invariant, signifying the mirror-protected TCIs. As such, we provide a concrete and quantitative recipe to determine the electronic topology of systems with mirror but without translational symmetry. Interestingly, a previously proposed aperiodic QSH state [54,55], which is based on (s, p_x, and p_y) orbitals in a Penrose-type quasicrystal, is also characterized by $B_m = 1$ in addition to the spin Bott index $B_s = 1$. Such a dual topological characteristic [70] is due to the essential equivalence of the mirror operator and the spin operator in such special systems.

For the quasicrystal in Fig. 1(b), we found that $B_m = 2$, indicating that it is indeed a TCI. According to the bulk-edge correspondence, it is not surprising that the nonzero mirror Bott index is consistent with the above-mentioned robust edge states. Moreover, $B_m = 2$ dictates that there exist two pairs of counterpropagating edge states within the energy gap. They move in the same (opposite) direction with identical (opposite) mirror eigenvalues. Different from periodic systems where the number of edge states can be easily counted from a ribbon calculation with two open boundaries, it is difficult to determine the number of midgap edge states from the spectrum of aperiodic systems with OBC. However, their edge states still lead to a quantized conductance of $2e^2/h$ per edge in the ballistic limit.

To verify the quantized conductance of the edge states in the aperiodic TCI, we further studied its transport properties by coupling it to two semi-infinite periodic leads with two open side boundaries, which host the edge states. In Fig. 2(a), we plot the two-terminal conductances which are calculated using the nonequilibrium Green's function method [71–73]. Remarkably, there is an obvious plateau of conductance at the quantized value $G = 4e^2/h$ for the two-terminal device, consistent with the calculated mirror Bott index. As shown in Fig. 2(b), the local density of state of the central quasicrystal at $E = 0$ eV [the blue star marked in Fig. 2(a)] mainly distributes on two edges of the quasicrystal, confirming that the conductive channels are mostly contributed by the topological edge states.

Unlike helical edge states in QSH insulators, the edge states in aperiodic TCIs are protected solely by the mirror symmetry $M_z : z \to -z$, but not time reversal. This leads to a remarkable consequence: applying a perpendicular electric field $\mathbf{E}$, which breaks the mirror symmetry, will open an energy gap in the edge states. To illustrate this effect and estimate its magnitude, we simulated the quasicrystal under a uniform perpendicular electric field with $H_{el}^z = Ez$ [74]. Because the electric field distorts the orbitals (especially the p_z orbital) along the z axis [see Fig. 2(c)], extra sp-like intersite hoppings are induced between p_z and $p_{x,y}$ orbitals [75]. The effective hopping strength is estimated as $\xi = \langle p_x|Ez|p_z, \mathbf{e}_x\rangle$, which represents the relative strength of the electric field (for a detailed discussion, see Supplemental Material [53]). We found that the midgap edge states, which are gapless in the OBC spectrum originally, are gapped in the presence of a weak perpendicular electric field, as shown in Fig. 2(d). Correspondingly, the transport calculation shows a gapped region with zero conductance under an electric field of $\xi = 3.75 \times 10^{-2}$ eV [see Fig. 2(a)], indicating that the edge modes are destroyed by the field-induced mirror symmetry breaking. In contrast, a magnetic field or internal magnetism is required to gap helical edge states of QSH insulators, which can be difficult to achieve. Thus, the tunability of the edge states in the aperiodic TCI provides a possible realization of topological transistors with high ON/OFF ratio [32].

Interestingly, by further increasing the perpendicular electric field, the bulk energy gap decreases to zero and

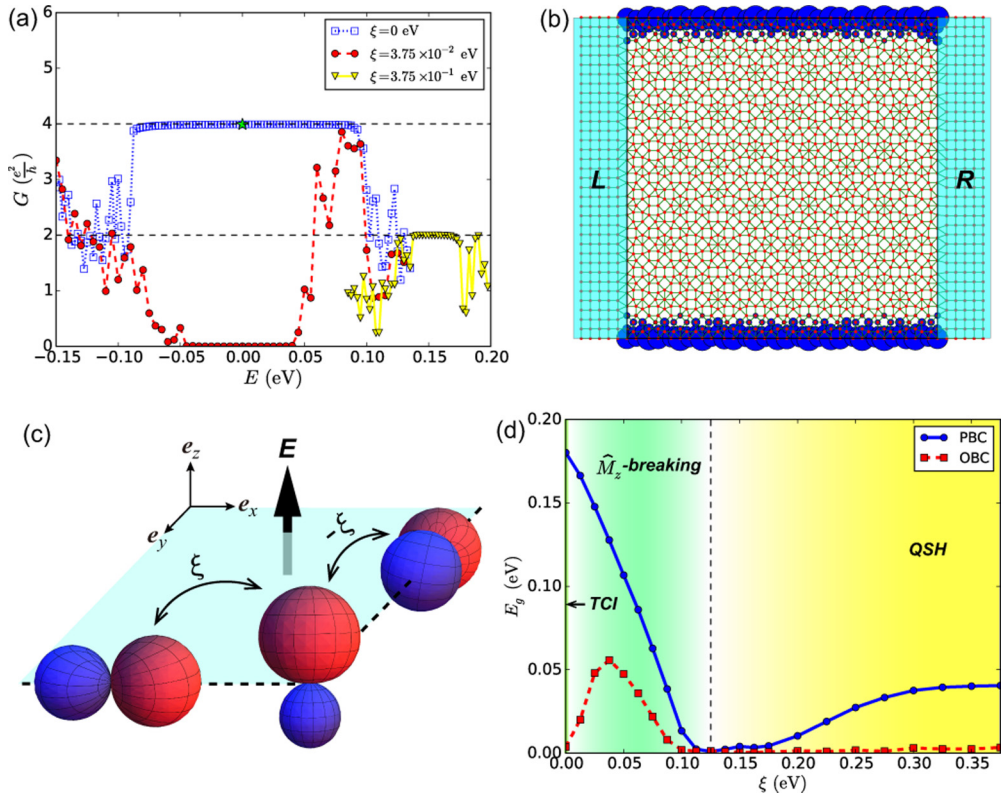

FIG. 2. (a) Two-terminal conductance G as a function of the Fermi energy E for quasicrystals with different perpendicular electric fields. (b) Local density of state $\rho_i(E)$ at $E = 0$ eV [marked as the green star in (a)] for the central quasicrystal in the transport simulation without perpendicular electric fields ($\xi = 0$ eV). The size of blue dot represents the relative value of local density of state. (c) Schematic illustration of the effect of a perpendicular electric field. ξ indicates the field-induced coupling between $p_{x,y}$ and p_z orbitals. (d) Topological phase transition induced by the perpendicular electric field.

reopens; meanwhile the OBC spectrum becomes nearly gapless simultaneously, as shown in Fig. 2(d). This actually implies a possible topological phase transition. We calculated the spin Bott index of the system with the reopened gap and found $B_s = 1$, indicating that the quasicrystal is indeed driven to a QSH state. Correspondingly, the OBC system under a strong electric field shows midgap edge states which are located on the boundary of the finite sample, confirming also its nontrivial topology. Furthermore, the transport simulation shows a clear plateau of $G = 2e^2/h$ for the quasicrystal in the QSH phase ($\xi = 3.75 \times 10^{-1}$ eV), as displayed in Fig. 2(a). Thus, applying an electric field can not only destroy the topological edge states of the aperiodic TCI to turn off the conductivity, but also drive the system into a new topological state with a different quantized conductance [76].

Such a topological phase transition from a TCI to a QSH insulator can be intuitively explained as follows: with the increasing electric field, the distorted p_z orbital becomes more and more asymmetric, and then the distorted p_z-$p_{x,y}$ band inversion resembles an s-$p_{x,y}$ PBI gradually. Consequently, the system is driven from a TCI to a QSH state. An alternative view is that the p_z-$p_{x,y}$ band inversion can be considered as two copies of s-$p_{x,y}$ PBI with opposite phases. The interaction between them is strictly forbidden by the mirror symmetry which guarantees the gapless topological edge states. Applying a perpendicular electric field, which breaks the mirror symmetry, hybridizes edge states stemming from the two PBIs and induces a gap in the OBC spectrum. Owing to the strong distortion of the p_z orbital with the increasing electric field [see Fig. 2(c)], one copy of the PBI is diminished and re-inverted back to the normal band order, while the other is enhanced and dominates the band topology of the system, inducing the topological phase transition. Physically, a Rashba SOC arises due to the perpendicular electric field. Different from the intrinsic SOC that remains a constant strength, the increasing Rashba SOC splits the bands, closes the energy gap, and eventually induces an extra PBI [77,78], which leads to a topological phase transition. Similar behaviors of the Rashba effect are also observed in crystalline counterparts of the aperiodic TCI [53].

Additionally, in order to test the robustness of the aperiodic TCI state and study its localization properties, we investigate the disorder effect on the Hamiltonian by adding an extra term, $W \sum_{i\alpha} \zeta_i c^\dagger_{i\alpha} c_{i\alpha}$, where ζ_i draws randomly for each site from the uniform distribution $[-1, 1]$ and W is the strength of disorder (see Supplemental Material [53]). As shown in top panel of Fig. 3(a), with the increasing W, the nontrivial energy gap of the aperiodic TCI decreases and disappears eventually. Due to Anderson localization, the disorder-induced gapless phase is not necessarily a metallic state as seen from band theory, but may turn out to be insulating. We checked the localization of each state by calculating its participation

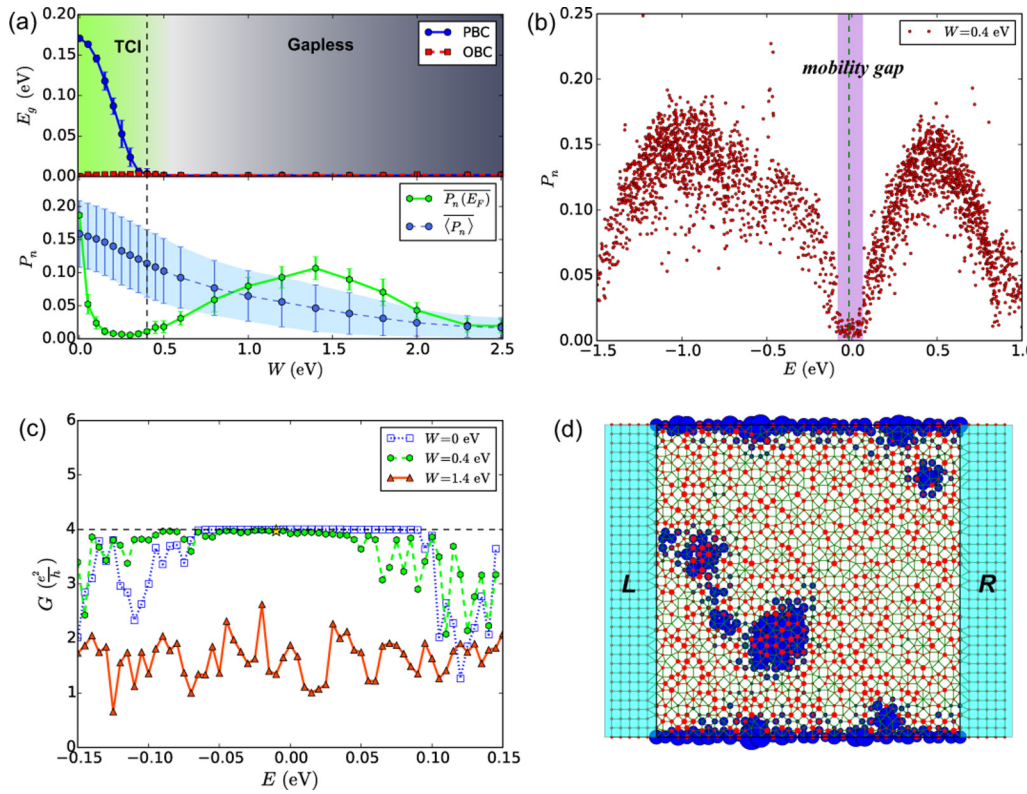

FIG. 3. (a) Energy gap E_g (top) and participation ratio $P_n(E)$ (bottom) as a function of disorder strength W for the quasicrystal. (b) Distribution of participation ratio $P_n(E)$ for a disordered quasicrystal with $W = 0.4$ eV. (c) Two-terminal conductance G as a function of the Fermi energy E for the quasicrystal without and with disorder. (d) The local density of state $\rho_i(E)$ at $E = -0.01$ eV [marked as the red star in (c)] for the disordered quasicrystal studied in the transport simulation. The size of red and blue dot represents the random on-site disorder and the relative value of local density of state $\rho_i(E)$, respectively.

ratio [79],

$$P_n(E) = \frac{(\sum_{i=1}^{N} |\langle i|\psi_n\rangle|^2)^2}{N \sum_{i=1}^{N} |\langle i|\psi_n\rangle|^4} \delta(E - E_n), \tag{9}$$

where $|\psi_n\rangle$ is the nth wave function with the corresponding eigenenergy E_n, and $\{|i\rangle\}$ is the local orbital base. By tracing the evolution of average participation ratio $\overline{\langle P_n \rangle}$ over the whole spectrum and $\overline{P_n(E_F)}$ around the Fermi level [see bottom panel of Fig. 3(a)], we found that a mobility gap opens to separate the relatively extended states in the disorder-induced gapless phase [80], as shown in Fig. 3(b). Hence, the disordered quasicrystal is still insulating and the aperiodic TCI phase is expected to persist. As shown in Fig. 3(c), the conductance of the disordered quasicrystal ($W = 0.4$ eV), which is mainly contributed by the robust topological edge states [see Fig. 3(d)], exhibits nearly quantized values within the energy window of the mobility gap. Therefore, the aperiodic TCI is robust against the effect of disorder persistent within the mobility gap induced by Anderson localization.

In conclusion, we have proposed the concept and an example of the aperiodic TCI phase in an octagonal quasicrystal. The nontrivial electronic topology is attributed to a mirror band inversion and characterized by a nonzero mirror Bott index, in addition to conventional evidences such as metallic edge states and quantized conductances. Although our work is based on a specific tiling, symmetry class, and orbital types, the notion of aperiodic TCI phases is generally applicable providing interesting future directions for research. Beyond the mirror-protected TCI phases, searching for new topological phases in quasicrystals is still ongoing; whether quasicrystals can host novel states with properties not found in crystals is an open question. For instance, due to the lack of classic crystallographic restriction, quasicrystals exhibit rotational symmetries that are forbidden in crystals, which raises the question of whether these symmetries can lead to new types of TCI phases. If so, the resulting TCI phases would only be feasible in aperiodic quasicrystals.

Note added. Recently, we become aware of another work [81] studying topological phases in an octagonal quasicrystal.

This work was supported by U.S. DOE-BES (Grant No. DE-FG02-04ER46148). This research used resources of the CHPC at the University of Utah and the National Energy Research Scientific Computing Center, a DOE Office of Science User Facility supported by the Office of Science of the U.S. Department of Energy under Contract No. DE-AC02-05CH11231.

[1] L. Fu, Phys. Rev. Lett. **106**, 106802 (2011).
[2] M. Z. Hasan and C. L. Kane, Rev. Mod. Phys. **82**, 3045 (2010).
[3] X.-L. Qi and S.-C. Zhang, Rev. Mod. Phys. **83**, 1057 (2011).
[4] A. Bansil, H. Lin, and T. Das, Rev. Mod. Phys. **88**, 021004 (2016).
[5] C. Fang, M. J. Gilbert, and B. A. Bernevig, Phys. Rev. B **86**, 115112 (2012).
[6] C. Fang, M. J. Gilbert, and B. A. Bernevig, Phys. Rev. B **87**, 035119 (2013).
[7] C.-K. Chiu, H. Yao, and S. Ryu, Phys. Rev. B **88**, 075142 (2013).
[8] T. Morimoto and A. Furusaki, Phys. Rev. B **88**, 125129 (2013).
[9] R.-J. Slager, A. Mesaros, V. Juričić, and J. Zaanen, Nat. Phys. **9**, 98 (2013).
[10] A. Alexandradinata, C. Fang, M. J. Gilbert, and B. A. Bernevig, Phys. Rev. Lett. **113**, 116403 (2014).
[11] K. Shiozaki and M. Sato, Phys. Rev. B **90**, 165114 (2014).
[12] H. Song, S.-J. Huang, L. Fu, and M. Hermele, Phys. Rev. X **7**, 011020 (2017).
[13] S.-J. Huang, H. Song, Y.-P. Huang, and M. Hermele, Phys. Rev. B **96**, 205106 (2017).
[14] H. C. Po, A. Vishwanath, and H. Watanabe, Nat. Commun. **8**, 50 (2017).
[15] T. Zhang, Y. Jiang, Z. Song, H. Huang, Y. He, Z. Fang, H. Weng, and C. Fang, Nature (London) **566**, 475 (2019).
[16] F. Tang, H. C. Po, A. Vishwanath, and X. Wan, Nature (London) **566**, 486 (2019).
[17] M. Vergniory, L. Elcoro, C. Felser, N. Regnault, B. A. Bernevig, and Z. Wang, Nature (London) **566**, 480 (2019).
[18] T. H. Hsieh, H. Lin, J. Liu, W. Duan, A. Bansil, and L. Fu, Nat. Commun. **3**, 982 (2012).
[19] Y. Ando and L. Fu, Annu. Rev. Condens. Matter Phys. **6**, 361 (2015).
[20] P. Dziawa, B. J. Kowalski, K. Dybko, R. Buczko, A. Szczerbakow, M. Szot, E. Łusakowska, T. Balasubramanian, B. M. Wojek, M. H. Berntsen, O. Tjernberg, and T. Story, Nat. Mater. **11**, 1023 (2012).
[21] T. Liang, Q. Gibson, J. Xiong, M. Hirschberger, S. P. Koduvayur, R. Cava, and N. Ong, Nat. Commun. **4**, 2696 (2013).
[22] Y. Okada, M. Serbyn, H. Lin, D. Walkup, W. Zhou, C. Dhital, M. Neupane, S. Xu, Y. J. Wang, R. Sankar, F. Chou, A. Bansil, M. Z. Hasan, S. D. Wilson, L. Fu, and V. Madhavan, Science **341**, 1496 (2013).
[23] S.-Y. Xu, C. Liu, N. Alidoust, M. Neupane, D. Qian, I. Belopolski, J. Denlinger, Y. Wang, H. Lin, L. A. Wray *et al.*, Nat. Commun. **3**, 1192 (2012).
[24] Y. Tanaka, T. Shoman, K. Nakayama, S. Souma, T. Sato, T. Takahashi, M. Novak, K. Segawa, and Y. Ando, Phys. Rev. B **88**, 235126 (2013).
[25] M. Kargarian and G. A. Fiete, Phys. Rev. Lett. **110**, 156403 (2013).
[26] M. Kindermann, Phys. Rev. Lett. **114**, 226802 (2015).
[27] H. Weng, J. Zhao, Z. Wang, Z. Fang, and X. Dai, Phys. Rev. Lett. **112**, 016403 (2014).
[28] T. H. Hsieh, J. Liu, and L. Fu, Phys. Rev. B **90**, 081112(R) (2014).
[29] T. Kawakami, T. Okamura, S. Kobayashi, and M. Sato, Phys. Rev. X **8**, 041026 (2018).
[30] Y. Kim, C. L. Kane, E. J. Mele, and A. M. Rappe, Phys. Rev. Lett. **115**, 086802 (2015).
[31] X. Li, F. Zhang, Q. Niu, and J. Feng, Sci. Rep. **4**, 6397 (2014).
[32] J. Liu, T. H. Hsieh, P. Wei, W. Duan, J. Moodera, and L. Fu, Nat. Mater. **13**, 178 (2014).
[33] J. Liu, X. Qian, and L. Fu, Nano Lett. **15**, 2657 (2015).
[34] H. Ozawa, A. Yamakage, M. Sato, and Y. Tanaka, Phys. Rev. B **90**, 045309 (2014).
[35] E. O. Wrasse and T. M. Schmidt, Nano Lett. **14**, 5717 (2014).
[36] C. Niu, P. M. Buhl, G. Bihlmayer, D. Wortmann, S. Blügel, and Y. Mokrousov, Nano Lett. **15**, 6071 (2015).
[37] C. Niu, P. M. Buhl, G. Bihlmayer, D. Wortmann, Y. Dai, S. Blügel, and Y. Mokrousov, Phys. Rev. B **95**, 075404 (2017).
[38] C.-H. Hsu, Z.-Q. Huang, C. P. Crisostomo, L.-Z. Yao, F.-C. Chuang, Y.-T. Liu, B. Wang, C.-H. Hsu, C.-C. Lee, H. Lin *et al.*, Sci. Rep. **6**, 18993 (2016).
[39] T. Janssen, G. Chapuis, and M. De Boissieu, *Aperiodic Crystals: From Modulated Phases to Quasicrystals: Structure and Properties* (Oxford University Press, Oxford, 2018).
[40] E. M. Barber, *Aperiodic Structures in Condensed Matter: Fundamentals and Applications* (CRC Press, Boca Raton, FL, 2008).
[41] T. Janssen, Acta Crystallogr., Sect. A: Found. Adv. **68**, 667 (2012).
[42] T. Harman and I. Melngailis, in *Applied Solid State Science* (Elsevier, New York, 1974), Vol. 4, pp. 1–94.
[43] B. A. Volkov and O. A. Pankratov, Pis'ma Zh. Eksp. Teor. Fiz. **42**, 145 (1985) [JETP Lett. **42**, 178 (1985)].
[44] O. Pankratov, S. Pakhomov, and B. Volkov, Solid State Commun. **61**, 93 (1987).
[45] B. A. Bernevig, T. L. Hughes, and S.-C. Zhang, Science **314**, 1757 (2006).
[46] H. Huang, Y. Xu, J. Wang, and W. Duan, WIRES: Comput. Mol. Sci. **7**, e1296 (2017).
[47] L. Fu and C. L. Kane, Phys. Rev. B **76**, 045302 (2007).
[48] B. Grünbaum and G. C. Shephard, *Tilings and Patterns* (W. H. Freeman and Company, New York, 1987).
[49] F. P. M. Beenker, *Algebraic Theory of Non-Periodic Tilings of the Plane by Two Simple Building Blocks: A Square and a Rhombus* (Eindhoven University of Technology Eindhoven, The Netherlands, 1982).
[50] M. Duneau, R. Mosseri, and O. Christophe, J. Phys. A: Math. Gen. **22**, 4549 (1989).
[51] J. C. Slater and G. F. Koster, Phys. Rev. **94**, 1498 (1954).
[52] W. A. Harrison, *Electronic Structure and the Properties of Solids: The Physics of the Chemical Bond* (Courier Corporation, North Chelmsford, MA, 2012).
[53] See Supplemental Material at http://link.aps.org/supplemental/10.1103/PhysRevB.101.041103 for more details about theoretical analysis, tight-binding models, and numerical results, which includes Refs. [82–96].
[54] H. Huang and F. Liu, Phys. Rev. Lett. **121**, 126401 (2018).
[55] H. Huang and F. Liu, Phys. Rev. B **98**, 125130 (2018).
[56] H. Huang and F. Liu, Phys. Rev. B **100**, 085119 (2019).
[57] J. C. Y. Teo, L. Fu, and C. L. Kane, Phys. Rev. B **78**, 045426 (2008).
[58] J. Bellissard, A. van Elst, and H. Schulz-Baldes, J. Math. Phys. (NY) **35**, 5373 (1994).
[59] R. Exel and T. A. Loring, J. Funct. Anal. **95**, 364 (1991).
[60] A. Kitaev, Ann. Phys. (NY) **321**, 2 (2006).

[61] R. Bianco and R. Resta, Phys. Rev. B **84**, 241106(R) (2011).
[62] E. Prodan, J. Phys A: Math. Theor. **44**, 113001 (2011).
[63] E. Prodan, New J. Phys. **12**, 065003 (2010).
[64] M. B. Hastings and T. A. Loring, J. Math. Phys. (NY) **51**, 015214 (2010).
[65] T. A. Loring and M. B. Hastings, Europhys. Lett. **92**, 67004 (2011).
[66] H. Katsura and T. Koma, J. Math. Phys. **57**, 021903 (2016).
[67] Q. Niu, D. J. Thouless, and Y.-S. Wu, Phys. Rev. B **31**, 3372 (1985).
[68] K. Kudo, H. Watanabe, T. Kariyado, and Y. Hatsugai, Phys. Rev. Lett. **122**, 146601 (2019).
[69] For a better convergency of the numerical algorithm, we perform a singular value decomposition $A = Z\Sigma W^\dagger$ for $U_{\pm i}$ and $V_{\pm i}$, where Z and W are unitary and Σ is real and diagonal, and identify the "unitary part," the $tilde07EA = ZW^\dagger$ as the new projected position operators.
[70] T. Rauch, M. Flieger, J. Henk, I. Mertig, and A. Ernst, Phys. Rev. Lett. **112**, 016802 (2014).
[71] S. Datta, *Electronic Transport in Mesoscopic Systems* (Cambridge University Press, Cambridge, 1997).
[72] M. Büttiker, Phys. Rev. B **38**, 9375 (1988).
[73] H. Huang, Z. Wang, N. Luo, Z. Liu, R. Lü, J. Wu, and W. Duan, Phys. Rev. B **92**, 075138 (2015).
[74] C. R. Ast and I. Gierz, Phys. Rev. B **86**, 085105 (2012).
[75] K. V. Shanavas and S. Satpathy, Phys. Rev. Lett. **112**, 086802 (2014).
[76] J. Liu and L. Fu, Phys. Rev. B **91**, 081407(R) (2015).
[77] C. L. Kane and E. J. Mele, Phys. Rev. Lett. **95**, 146802 (2005).
[78] C. L. Kane and E. J. Mele, Phys. Rev. Lett. **95**, 226801 (2005).
[79] T. Odagaki and D. Nguyen, Phys. Rev. B **33**, 2184 (1986).
[80] Y.-Y. Zhang, R.-L. Chu, F.-C. Zhang, and S.-Q. Shen, Phys. Rev. B **85**, 035107 (2012).
[81] D. Varjas, A. Lau, K. Pöyhönen, A. R. Akhmerov, D. I. Pikulin, and I. C. Fulga, Phys. Rev. Lett. **123**, 196401 (2019).
[82] W. A. Harrison, Phys. Rev. B **24**, 5835 (1981).
[83] M. van Schilfgaarde and W. A. Harrison, Phys. Rev. B **33**, 2653 (1986).
[84] M. Kitamura and W. A. Harrison, Phys. Rev. B **44**, 7941 (1991).
[85] G. Grosso and C. Piermarocchi, Phys. Rev. B **51**, 16772 (1995).
[86] L. Shi and D. A. Papaconstantopoulos, Phys. Rev. B **70**, 205101 (2004).
[87] M. P. López Sancho, J. M. López Sancho, and J. Rubio, J. Phys. F **14**, 1205 (1984).
[88] M. P. López Sancho, J. M. López Sancho, and J. Rubio, J. Phys. F **15**, 851 (1985).
[89] Z. M. Stadnik, *Physical Properties of Quasicrystals* (Springer Science & Business Media, New York, 2012), Vol. 126.
[90] H.-R. Trebin, *Quasicrystals: Structure and Physical Properties* (Wiley, Weinheim, 2006).
[91] Y. Song, W. A. Atkinson, and R. Wortis, Phys. Rev. B **76**, 045105 (2007).
[92] J. Li, R.-L. Chu, J. K. Jain, and S.-Q. Shen, Phys. Rev. Lett. **102**, 136806 (2009).
[93] C. W. Groth, M. Wimmer, A. R. Akhmerov, J. Tworzydło, and C. W. J. Beenakker, Phys. Rev. Lett. **103**, 196805 (2009).
[94] N. Wang, H. Chen, and K. H. Kuo, Phys. Rev. Lett. **59**, 1010 (1987).
[95] J. C. Jiang, N. Wang, K. K. Fung, and K. H. Kuo, Phys. Rev. Lett. **67**, 1302 (1991).
[96] N. Wang, K. K. Fung, and K. Kuo, Appl. Phys. Lett. **52**, 2120 (1988).